doi:10.1093/brain/awh399 *Brain* (2005), **128**, 678–687

O-(2-[^{18}F]fluoroethyl)-L-tyrosine PET combined with MRI improves the diagnostic assessment of cerebral gliomas

Dirk Pauleit,[1,5] Frank Floeth,[6] Kurt Hamacher,[2,4] Markus J. Riemenschneider,[7] Guido Reifenberger,[7] Hans-Wilhelm Müller,[5] Karl Zilles,[3,4] Heinz H. Coenen[2,4] and Karl-Josef Langen[3,4]

[1]*Clinic for Nuclear Medicine (KME),* [2]*Institute of Nuclear Chemistry (INC),* [3]*Institute of Medicine (IME) and* [4]*Brain Imaging Center West, Research Center Jülich, Jülich,* [5]*Department of Nuclear Medicine,* [6]*Department of Neurosurgery and* [7]*Department of Neuropathology, Heinrich Heine University, Düsseldorf, Germany*

Correspondence to: Dirk Pauleit, Clinic for Nuclear Medicine (KME), Research Center Jülich, Leo-Brandt-Strasse; 52425 Jülich, Germany
E-mail: pauleit@web.de

Summary

MRI is commonly used to determine the location and extent of cerebral gliomas. We investigated whether the diagnostic accuracy of MRI could be improved by the additional use of PET with the amino acid *O*-(2-[^{18}F]fluoroethyl)-L-tyrosine (FET). In a prospective study, PET with FET and MRI was performed in 31 patients with suspected cerebral gliomas. PET and MRIs were co-registered and 52 neuronavigated tissue biopsies were taken from lesions with both abnormal MRI signal and increased FET uptake (match), as well as from areas with abnormal MR signal but normal FET uptake or vice versa (mismatch). Biopsy sites were labelled by intracerebral titanium pellets. The diagnostic performance for the identification of cellular tumour tissue was analysed for either MRI alone or MRI combined with FET PET using alternative free response receiver operating characteristic curves (ROCs). Histologically, 26 biopsy samples corresponded to cellular glioma tissue and 26 to peritumoral brain tissue. The diagnostic performance, as determined by the area under the ROC curve (Az), was Az = 0.80 for MRI alone and Az = 0.98 for the combined MRI and FET PET approach ($P < 0.001$). MRI yielded a sensitivity of 96% for the detection of tumour tissue but a specificity of only 53%, and combined use of MRI and FET PET yielded a sensitivity of 93% and a specificity of 94%. Combined use of MRI and FET PET in patients with cerebral gliomas significantly improves the identification of cellular glioma tissue and allows definite histological tumour diagnosis. Thus, our findings may have considerable impact on target selection for diagnostic biopsies as well as therapy planning.

Keywords: MRI; PET; FET; amino acid; glioma

Abbreviations: Az = area under the ROC curve; dwMRI = diffusion-weighted MRI; FDG = 2-[^{18}F]fluoro-2-deoxyglucose; FET = *O*-(2-[^{18}F]fluoroethyl)-L-tyrosine; FLAIR = fluid-attenuated inversion recovery; Gd = gadolinium; MET = L-methyl-[^{11}C]-methionine; ROC = receiver operating characteristic; ROI = region of interest

Received August 7, 2004. Revised November 10, 2004. Accepted December 22, 2004. Advance Access publication February 2, 2005

Introduction

MRI has evolved as the most important diagnostic tool for assessing brain neoplasm due to its excellent soft tissue contrast and multiplanar reconstruction capabilities (DeAngelis, 2001). However, studies investigating the accuracy of MRI in delineating the tumour boundaries of gliomas are scarce. Some studies used image-guided tumour biopsy or post-mortem specimens for correlation and reported on discrepancies between the real tumour extent and signal abnormalities in MRI (Watanabe *et al*., 1992; Jansen *et al*., 2000).

In contrast to MRI, metabolic imaging with PET has gained only a limited role in the diagnostic evaluation of gliomas. PET with 18F-fluorodeoxyglucose (FDG) may be useful in estimating tumour grade and prognosis of gliomas,

but the delineation of the tumour extent is difficult because of high glucose metabolism in the cerebral cortex (Wong *et al*., 2002). Encouraging reports of improved tumour delineation with PET have been reported using radiolabelled amino acids such as 11C-methionine (MET) (Bergstrom *et al*., 1983; Mosskin *et al*., 1987; Herholz *et al*., 1998; Kaschten *et al*., 1998). It was shown by stereotactic serial biopsies that the actual tumour size was better reflected by MET PET than by CT or MRI (Mosskin *et al*., 1989). Moreover, the method has been reported as helpful for the determination of the optimal biopsy site (Goldman *et al*., 1996; Pirotte *et al*., 2004). Due to the short physical half-life of the 11C label (20 min), however, MET PET remains restricted to a few PET centres with a cyclotron on site and could not be established in routine clinical practice despite convincing first clinical results.

FET is one of the first 18F-labelled amino acids that can be produced in large amounts for clinical purposes and is applicable for PET studies using a satellite concept similar to the widely used FDG (Wester *et al*., 1999; Hamacher *et al*., 2002). Although this amino acid is not incorporated into proteins, uptake by tumour cells is stereospecific and mediated by amino acid transporters (Heiss *et al*., 1999; Langen *et al*., 2003). Initial studies using FET PET for the analysis of human brain tumours and rat gliomas have shown results similar to those obtained with MET PET (Weber *et al*., 2000; Langen *et al*., 2003). Furthermore, effective biopsy target guidance of FET PET has been reported in two children with brain tumours in whom MRI was not conclusive (Messing-Jünger *et al*., 2002).

The purpose of our present study was to determine whether combined imaging with MRI and PET using the amino acid FET allows better distinction between cellular glioma tissue from unspecific peritumoral brain tissue. A reliable non-invasive distinction between tumour tissue and the peritumoral brain tissue would be very helpful for the planning of surgical resections, targeted biopsies and radiation therapy of cerebral gliomas. Neuronavigated biopsies and intraoperative markers were used to enable an exact correlation of the imaging findings with histological specimens.

Table 1 *Patient data*

Patient	Age	Sex	No. of labelled biopsies	Final histological diagnosis
1	36	F	2	Anaplastic oligoastrocytoma WHO grade III
2	2	F	1	Astrocytoma WHO grade II
3	45	F	3	Astrocytoma WHO grade II
4	10	M	1	Anaplastic astrocytoma WHO grade III
5	30	M	1	Pilocytic astrocytoma WHO grade I
6	66	F	2	Reactive astrogliosis
7	54	F	3	Astrocytoma WHO grade II
8	50	F	1	Anaplastic astrocytoma WHO grade III
9	7	M	1	Anaplastic oligodendroglioma WHO grade III
10	61	F	1	Glioblastoma WHO grade IV
11	25	F	1	Reactive astrogliosis
12	73	M	4	Glioblastoma WHO grade IV
13	23	F	1	Anaplastic astrocytoma WHO grade III
14	36	M	1	Anaplastic oligodendroglioma WHO grade III
15	53	F	2	Astrocytoma WHO grade II
16	13	F	1	Reactive astrogliosis
17	30	F	1	Pilocytic astrocytoma WHO grade I
18	67	M	2	Anaplastic astrocytoma WHO grade III
19	38	M	1	Astrocytoma WHO grade II
20	46	F	2	Anaplastic astrocytoma WHO grade III
21	57	F	3	Anaplastic oligodendroglioma WHO grade III
22	36	M	4	Astrocytoma WHO grade II
23	31	M	3	Anaplastic astrocytoma WHO grade III
24	49	F	2	Reactive astrogliosis
25	51	F	2	Reactive astrogliosis
26	74	F	1	Astrocytoma WHO grade II
27	58	F	4	Anaplastic oligoastrocytoma WHO grade III
28	58	F	1	Anaplastic oligodendroglioma grade WHO III

Material and methods

Patients

Thirty-one consecutive patients were included in this prospective study. All patients had space-occupying intracerebral lesions that on CT and MRI appeared as highly suspicious of cerebral gliomas and were therefore subjected to neuronavigated biopsy at the Department of Neurosurgery, Heinrich Heine University, Düsseldorf. None of the patients had undergone previous surgery, chemo- or radiotherapy. Three patients with no increased FET uptake were excluded from further analysis because histological analysis revealed ischaemic infarction in two patients and a demyelinating disease in the third patient. Thus, a total of 28 patients (19 female, nine male; mean age 42 ± 20 years) could be evaluated. The individual data of these patients are provided in Table 1. The study was approved by the university ethics committee and federal authorities. All subjects gave written informed consent for their participation in the study. Fiducial markers were fixed at the patients' head to allow the co-registration of MRI, PET and intraoperative data.

FET PET

The amino acid FET was produced via aminopolyether-activated nucleophilic 18F-fluorination of *N*-trityl-*O*-(2-tosyloxyethyl)-L-tyrosine tert-butylester and subsequent deprotection with a specific radioactivity of >200 GBq/μmol by optimizing the previous method (Hamacher *et al*., 2002). The uncorrected radiochemical yield was about 35% and radiochemical purity >98%. The tracer was administered as isotonic neutral solution.

Since FET accumulates in tumour tissue and normal brain tissue within 15 min after injection and remains relatively stable thereafter

(Weber *et al*., 2000), PET studies were acquired 15–40 min after intravenous injection of 200 MBq FET. The measurements were performed on an Ecat Exact HR+ scanner in 3D mode (Siemens Medical Systems, Hoffman Estates, IL, USA; 32 rings, axial field of view 15.5 cm). For attenuation correction, transmission scans with three 68Ge/68Ga rotating line sources were measured. After correction for random and scattered coincidences as well as dead time, image data were obtained by filtered back-projection in Fourier space using the Ecat 7.2 software [direct inverse Fourier transformation, Shepp filter 2.48 mm (full width half maximum), pixel size 2 × 2 × 2.4 mm^3]. The reconstructed images were decay-corrected; the reconstructed image resolution was about 5.5 mm. 68Ge markers were used as fiducial markers.

MRI

On the same day MRI examinations were performed in a 1.5 tesla MRI scanner (Sonata; Siemens, Erlangen, Germany) with a standard head coil and disposable MRI markers (BrainLab, Heimstetten, Germany). The MRI protocol consisted of a T1-weighted 3D-MPRAGE (magnetization prepared rapid acquisition gradient echo) sequence (field of view 25 cm, matrix 205 × 256, repetition time 2200 ms, echo time 3.9 ms, inversion time 1200 ms, flip angle 15°, number of slices 128, slice thickness 1.5 mm, slice gap 0 mm, number of averages 1, time of acquisition 6:38 min) before and 2 min after injection of 20 ml Gd-DTPA (Magnevist, Schering, Germany) and a transverse FLAIR (fluid attenuation inversion recovery) sequence (field of view 25 cm, matrix 205 × 256, repetition time 9000 ms, echo time 119 ms, inversion time 2500 ms, flip angle 90°, number of slices 25, slice thickness 5 mm, slice gap 0 mm, number of averages 2, time of acquisition 4 min 32 seconds).

Neuronavigated biopsies

Neuronavigated biopsies were performed at the Department of Neurosurgery one to three days after FET PET and MRI. Co-registered FET PET and MRI were transferred to the neuronavigation system (Vector Vision, BrainLab, Heimstetten, Germany) using the fiducial markers. Biopsies were taken from 'matched' lesions with both increased MR signal on the FLAIR sequence and increased FET uptake, as well as from 'mismatch' areas with increased MR signal on the FLAIR sequence but normal FET uptake or increased FET uptake and normal MR signal on the FLAIR sequence. The biopsy sites were selected under the responsibility of the neurosurgeon with the premise that a benefit for the individual patient could be expected and that the procedure did not significantly increase the risk of adverse effects. Increased signal intensity on the FLAIR sequence and increased FET uptake were defined as the signal or uptake that exceeds the mean of the normal brain by more than three standard deviations, as determined by ROI (region of interest) analysis.

A 2 mm stereotactic forceps was used and a total of 52 neuroradiologically defined biopsies were taken. Biopsy sites were labelled by intracerebral titanium pellets (MHT Medical High Tech, Bad Krozingen, Germany) and confirmed by postoperative imaging (Figs 1 and 2).

Histology

Each biopsy was investigated intraoperatively by a neuropathologist using haematoxylin-eosin-stained smear preparations. However, the final histological assessment was carried out on routine histological sections after formalin fixation and paraffin embedding of the biopsy specimens. Tumour type and malignancy grade of each tumour was determined according to the Word Health Organization (WHO) classification of tumours of the nervous system (Kleihues *et al*., 2002) using conventional staining (haematoxylin and eosin, reticulin stain), as well as immunohistochemical staining for glial fibrillary acidic protein (GFAP), the macrophage/microglia marker CD68 and the proliferation marker Ki-67 (MIB1). In a separate session, all biopsy specimens from the patients included in this study were histologically reassessed by two neuropathologists in consensus, who were blinded to the imaging results. During this session, each specimen was assigned to either of two categories: (i) cellular glioma tissue that was classified and graded according to WHO criteria, or (ii) peritumoral brain tissue that showed diagnostically unspecific reactive changes, such as oedema, astrogliosis and microglial activation.

Data analysis

Preoperative MRI, FET PET and postoperative imaging were co-registered using dedicated software (MPI tool version 3.28; ATV, Kerpen, Germany). Standardized ROIs with a size of 25 mm^2 were placed manually at the biopsy sites centred to the titanium pellets on postoperative images. These ROIs were copied to the co-registered preoperative PET and MRIs for quantitative analysis. In addition, similar-size ROIs were placed in analogous regions in the contralateral hemisphere so that a corresponding mirror image location was available in the normal appearing brain. For the calculation of the lesion-to-brain ratio the mean ROI value of the lesion was divided by the mean ROI value of the normal brain in the FET PET scan (FET ratio), non-enhanced T1-weighted MR sequences (T1 ratio), the gadolinium-enhanced T1-weighted MR sequences (Gd-T1 ratio) and the FLAIR sequences (FLAIR ratio). The non-parametric *U*-test of Mann and Whitney was used for statistical comparison of the lesion-to-brain ratios between the different imaging modalities and the Kruskal–Wallis test for the comparison of tumour-to-brain ratios and WHO grading. Binary logistic regression analysis was performed to analyse whether FET PET is an independent predictor of the presence of tumour tissue in addition to MRI.

Alternative free response ROC analysis, which reflects rather closely the decision process in routine clinical practice, was used to determine the diagnostic accuracy of MRI alone versus the combination of MRI and FET PET. Since MRI with detailed anatomical information is essential for brain tumour operations, a separate analysis of FET PET alone, i.e. without MRI, was not performed. Co-registered MRIs (non-enhanced T1-weighted MR sequences, gadolinium-enhanced T1-weighted MR sequences and T2-weighted FLAIR sequence) and co-registered MRI/FET PET images were presented separately to three independent external observers (one experienced consultant in neuroradiology, one in neurosurgery, and one in nuclear medicine). The ROC analysis included 52 lesions with imaging abnormalities that were confirmed by histopathology. Since no biopsies from normal brain tissue were available, 28 brain areas (one in each patient) that showed no changes on MRI and FET PET images were additionally defined as non-tumorous tissue by one neurosurgeon and one radiologist in consensus, neither of whom took part in the ROC analysis. The reviewing procedure in the ROC analysis was assessed in two sessions; the images were randomly assigned to each observer, who had

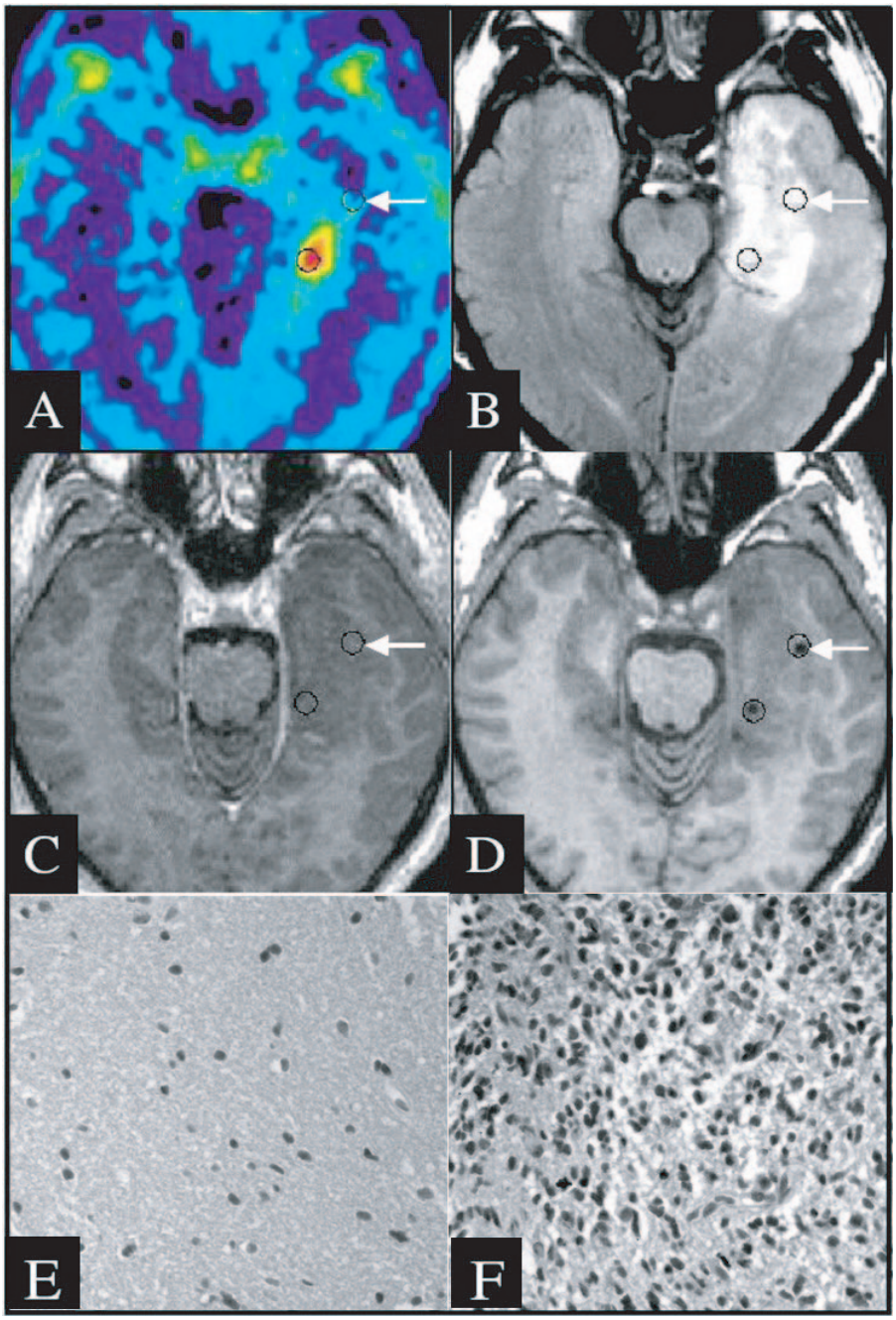

Fig. 1 FET PET, co-registered MRIs and histology of the biopsy samples in patient 23 diagnosed with an anaplastic astrocytoma of WHO grade III. MRI showed no enhancement of Gd-DTPA and distinction of tumour tissue and peritumoral brain tissue is difficult on the MRIs. PET revealed a circumscribed increase in uptake of the amino acid FET within the large area of abnormal MR signal intensities. (**A**) FET PET. (**B**) FLAIR sequence. (**C**) Gd-enhanced T1-weighted sequence. (**D**) Postoperative T1-weighted sequence with titanium markers at the biopsy sites. (**E**) Histology of the biopsy sample marked by the arrow showing peritumoral tissue with oedema and reactive astrogliosis (haematoxylin and eosin) (corresponding FET ratio, 1.1; T1 ratio, 0.8; Gd-T1 ratio, 0.9; FLAIR ratio, 1.5). (**F**) Histology of the biopsy sample marked by the circle without an arrow showing a cellular glioma corresponding to an anaplastic astrocytoma of WHO grade III (haematoxylin and eosin) (corresponding FET ratio, 2.7; T1 ratio, 0.9, Gd-T1 ratio, 0.9; FLAIR ratio, 1.2).

no knowledge of the clinical information. In the first session, the observers reviewed the co-registered MRIs, including all MR sequences, and in the second session MRIs and FET PET images were presented to the observers for scoring. Each observer assigned each marked lesion to a confidence rating score on the basis of a six-point rating scale as follows: 6, definitely positive; 5, probably positive; 4, possibly positive; 3, possibly negative; 2, probably negative; 1, definitely negative for tumour tissue. For the determination of the sensitivity, specificity and accuracy, a rating score of 4 or greater was considered positive for tumour tissue.

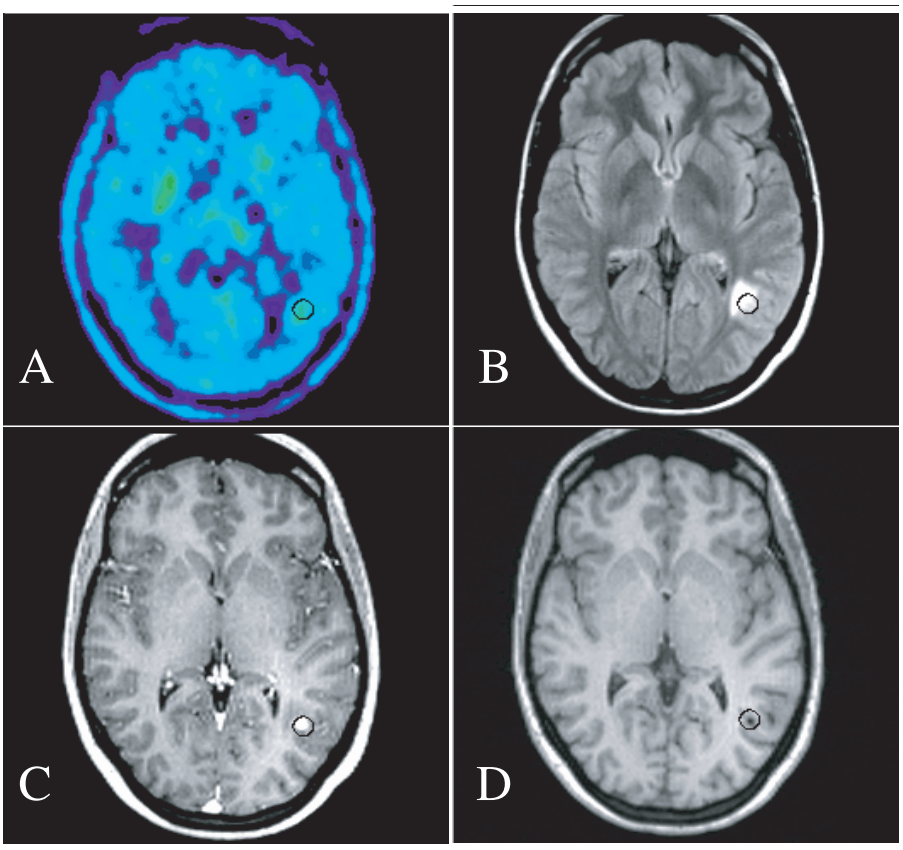

Fig. 2 FET PET and co-registered MRIs in patient 11. MRI showed increased MR signal on the T2-weighted FLAIR sequence and focal enhancement of Gd-DTPA. No increased FET uptake could be identified on PET images and histology revealed astrogliosis only (corresponding FET ratio, 1.2; T1 ratio, 0.9; Gd-T1 ratio, 1.5; FLAIR ratio, 1.9). (**A**) FET PET. (**B**) FLAIR sequence. (**C**) Gd-enhanced T1-weighted sequence. (**D**) Postoperative T1-weighted sequence with the titanium marker at the biopsy site.

Composite ROC curves were used to represent the performance of all observers as a group and were calculated by averaging the scores assigned by each of the observers. The κ statistic was used to measure the degree of agreement among the observers; κ values between 0 and 0.20 were considered to indicate a positive slight correlation, between 0.21 and 0.40 fair correlation, between 0.41 and 0.60 good correlation, between 0.61 and 0.80 very good correlation; and greater than 0.80 excellent correlation.

Alternative free response ROC curves were generated for MRI and for the combined use of MRI and FET PET. The diagnostic accuracies of MRI alone and that of the combined use of MRI and FET PET were determined by calculating the area under the ROC curve (Az) using dedicated ROC evaluation software (Rockit 0.9B; C. Metz, University of Chicago, Chicago, IL, USA). Differences between ROC curve integrals were tested for significance by using the two-tailed area test (a univariate *Z* score test of the difference between the areas under the ROC curves with the null hypothesis that the data sets arose from binomial ROC curves with equal areas beneath them). Probability values less than 0.05 were considered significant.

Results

Twenty-six of the 52 investigated biopsy specimens corresponded histologically to cellular tumour tissue that could be classified and graded according to WHO criteria (Table 2). The other 26 biopsy specimens showed diagnostically unspecific changes corresponding to peritumoral brain tissue with oedema and reactive gliosis. Biopsies taken from matched brain areas (MRI and FET PET positive, $n = 28$) revealed cellular tumour tissue in 24 instances (86%) and peritumoral tissue in only four instances (14%). Mismatched areas ($n = 24$) included 23 sites with increased signal on the FLAIR sequence but unsuspicious FET PET and one site with normal MRI but increased FET uptake. Histologically, biopsies from these mismatched areas revealed cellular tumour tissue in only three instances (12%) and peritumoral brain tissue in 21 instances (88%).

FET PET in tumour tissue and peritumoral tissue

The mean lesion-to-brain ratio of FET uptake was 2.6 ± 0.9 for the samples taken from tumour tissue and 1.2 ± 0.4 for the samples corresponding to peritumoral tissue ($P < 0.001$).

The FET ratio showed a trend towards higher FET ratios in high-grade tumours but no significant differences were identified for the FET ratios among the different WHO grades ($P = 0.123$).

Table 2 *Tumour-to-brain ratios and histological results of the biopsies*

Patient	Biopsy from		Tumour-to-brain ratio			Histology	
	Matched area	FET	T1	Gd-T1	FLAIR	Tumour tissue	WHO grading
1	Yes	1.2	0.8	0.8	2.2	No	–
1	No	2.1	0.9	0.9	1.7	No	–
2	Yes	1.7	1.0	1.0	1.2	No	–
3	Yes	2.2	0.9	1.0	2.0	Yes	II
3	Yes	2.4	0.8	0.8	2.1	Yes	II
3	No	1.6	0.9	0.9	1.8	No	–
4	Yes	3.1	0.8	1.5	1.2	Yes	III
5	Yes	4.2	0.7	1.1	1.7	Yes	II
6	No	1.0	0.9	0.8	2.2	No	–
6	No	0.5	1.0	0.9	2.0	No	–
7	Yes	3.0	0.6	0.7	2.0	Yes	II
7	Yes	3.7	0.7	0.7	1.9	Yes	II
7	No	1.1	0.6	0.6	1.8	Yes	II
8	No	0.9	0.5	0.5	1.5	Yes	III
9	Yes	4.4	1.0	1.3	1.3	Yes	III
10	Yes	1.9	0.8	0.8	1.6	No	–
11	No	1.2	0.9	1.5	1.9	No	–
12	Yes	1.0	1.0	1.0	1.0	No	–
12	Yes	2.9	1.5	1.8	2.5	Yes	IV
12	No	3.4	1.0	1.0	1.0	Yes	III
12	No	1.5	0.9	1.0	1.9	No	–
13	Yes	2.0	0.8	1.0	1.3	Yes	III
14	Yes	3.0	0.8	1.0	2.2	Yes	III
15	Yes	2.3	0.7	0.8	1.9	Yes	II
15	No	1.4	0.8	0.6	1.3	No	–
16	No	1.1	0.8	0.9	1.5	No	–
17	Yes	1.6	0.7	0.6	1.5	Yes	I
18	Yes	2.0	0.8	1.2	1.2	Yes	III
18	No	1.0	0.9	0.9	1.2	No	–
19	Yes	1.8	0.8	0.9	1.8	Yes	II
20	Yes	3.8	0.7	0.7	1.8	Yes	III
20	No	0.8	0.8	0.8	2.1	No	–
21	Yes	3.7	0.8	1.3	1.7	Yes	III
21	No	0.9	0.7	0.7	2.8	No	–
21	No	1.5	0.6	0.6	2.7	No	–
22	Yes	1.8	0.8	0.9	1.6	Yes	II
22	Yes	1.7	0.7	0.8	1.9	Yes	II
22	No	1.1	0.6	0.7	2.0	No	–
22	No	1.3	0.6	0.7	1.7	No	–
23	Yes	2.7	0.9	0.9	1.2	Yes	III
23	No	1.0	0.8	0.8	1.4	No	–
23	No	1.1	0.8	0.9	1.5	No	–
24	No	1.2	0.9	0.9	1.5	No	–
24	Yes	1.7	0.9	0.9	1.7	No	–
25	No	0.9	0.8	0.9	2.1	No	–
25	No	1.2	0.9	1.0	1.7	No	–
26	Yes	1.7	1.0	1.0	1.2	Yes	II
27	Yes	2.4	0.8	1.1	1.5	Yes	II
27	Yes	2.3	0.8	1.1	1.4	Yes	III
27	No	0.9	0.9	1.0	1.6	No	–
27	No	0.9	0.9	0.9	1.9	No	–
28	Yes	3.4	0.7	1.5	2.8	Yes	III

The sensitivity of the lesion-to-brain ratio of FET uptake for the detection of tumour tissue using a threshold for the FET ratio of 1.6 was 92% (24/26) and the specificity 81% (21/26). In 22 of the 24 (92%) mismatch areas FET PET predicted correctly the presence or absence of tumour tissue (Fig. 1).

MRI in tumour tissue and peritumoral tissue

The mean values of the lesion-to-brain ratios of the different MRI sequences revealed no significant difference for cellular tumour tissue and peritumoral brain tissue (Table 3).

Table 3 *Tumour-to-brain ratios for cellular glioma tissue and peritumoral brain tissue*

Tissue type	*n*	FET ratio	T1 ratio	Gd-T1 ratio	FLAIR ratio
Glioma	26	2.60 ± 0.93	0.81 ± 0.18	1.00 ± 0.31	1.65 ± 0.49
Peritumoral	26	1.24 ± 0.41	0.83 ± 0.11	0.88 ± 0.17	1.77 ± 0.43
Mann–Whitney *U*-test		$P < 0.0001$	$P = 0.11$	$P = 0.13$	$P = 0.40$

Table 4 *Coefficients of the binary logistic regression analysis*

	Coefficient	SD	Wald	*P*
FET ratio	5.67	1.95	8.49	0.004
T1 ratio	−13.08	6.83	3.67	0.06
Gd-T1 ratio	6.12	4.27	2.05	0.15
FLAIR ratio	−3.80	1.77	4.62	0.03
Constant	1.91			

When each MR sequence was considered separately, the sensitivity and the specificity of the non-enhanced T1-weighted sequence (threshold T1 ratio, 1.0) was 85% (22/26) and 12% (2/26), that of the Gd-enhanced T1-weighted sequence (threshold Gd-T1 ratio,1.0) was 38% (10/26) and 96% (25/26), and that of the FLAIR sequence (threshold FLAIR ratio, 1.0) was 96% (25/26) and 4% (1/26), respectively.

Eleven biopsies were taken from tumour areas with both increased signal intensity on the FLAIR sequence and contrast medium enhancement on Gd-enhanced T1-weighted images.

In 10 of these 11 biopsy samples tumour tissue was identified (two WHO grade II gliomas; seven WHO grade III gliomas, one WHO grade IV glioma). In one biopsy, histology revealed only reactive changes (Fig. 2).

Binary logistic regression analysis

In the logistic regression analysis using all lesion-to-brain ratios (FET ratio, T1 ratio, Gd-T1 ratio and FLAIR ratio) the FET ratio was identified as an independent significant ($P = 0.004$) coefficient for the distinction of tumour tissue and peritumoral tissue. The calculated variables in this logistic regression model are given in Table 4.

ROC analysis

The calculated area under the alternative free response ROC curve (Az) using MRI alone as the diagnostic test was Az = 0.80 and that for the combined use of MRI and FET PET was Az = 0.98 ($P < 0.001$). The ROC curves (pooled data of three observers) are shown in Fig. 3.

When a rating of the six-point rating scale of 1–3 was considered negative and a rating of 4 or higher was considered positive for cellular tumour tissue, the sensitivity of MRI alone was 96%, but specificity was only 53% (accuracy 68%). Combined use of MRI and FET PET yielded a similar sensitivity of 93% but a substantially improved specificity of 94% (accuracy 94%).

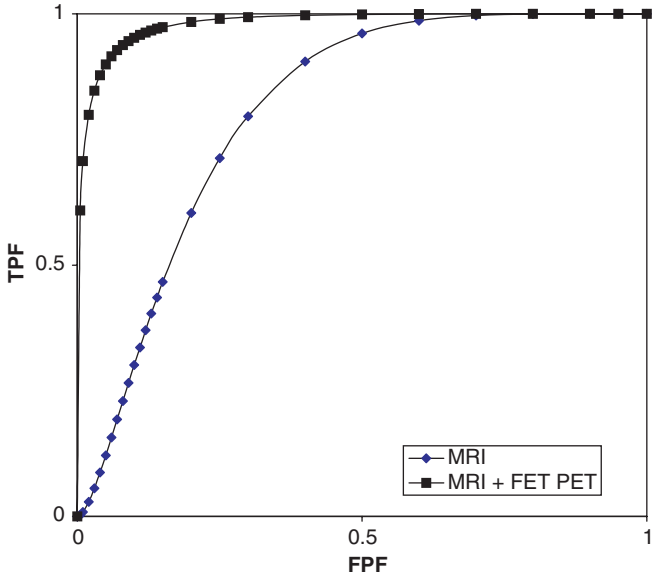

Fig. 3 Composite ROC curves for the three independent observers. The calculated area under the alternative free response ROC curve (Az) for the combined use of MRI and FET PET was Az = 0.98 and that for MRI alone was Az = 0.80. Observers were significantly ($P < 0.001$) more accurate in the distinction of tumour tissue and peritumoral brain tissue with MRI and FET PET than with MRI alone.

The determination of interobserver variability for the six-point-scale yielded only weak agreement for MRI with a mean κ value of 0.25 ± 0.09 (range 0.17–0.34) and good agreement for combined interpretation of MRI and FET PET, with a mean κ value of 0.51 ± 0.10 (range 0.40–0.60).

When considering only the presence or absence of cellular tumour (negative: a rating of 1–3; positive: a rating of 4 or higher), the agreement among the observers was very good (mean κ value, 0.68 ± 0.11) for MRI and excellent (mean κ value, 0.95 ± 0.03) for combined analysis of MRI and FET PET.

Discussion

Our results suggest that the combined use of MRI and FET PET is superior to that of MRI alone for the non-invasive distinction of tumour tissue and peritumoral brain tissue in patients with cerebral gliomas.

In this prospective study, neuronavigated biopsies were taken from matched and mismatched brain areas after imaging with MRI and PET using the new 18F-labelled amino acid FET. The biopsy sites were marked by intracerebral titanium pellets, which enabled a comparison of co-registered MRI and FET PET data with those of histological specimens with the highest precision that can be achieved.

In the ROC analysis, performed by three external independent observers, diagnostic accuracy was significantly improved when FET PET was used in addition to MRI. This was mainly caused by the increase of specificity from 53% using MRI alone, compared with 94% by the combined interpretation of MRI and FET PET data.

The lesion-to-brain ratio of FET uptake was an independent significant predictor for the distinction of tumour tissue and peritumoral tissue. The rate of positive results for tumour tissue in lesions with both increased signal intensity on FLAIR sequences and increased FET uptake was about 88% compared with 12% in mismatched brain areas.

Data comparing the accuracy of MRI and the delineation of tumour boundaries in gliomas are sparse (for review see Kelly *et al*., 1987; Johnson *et al*., 1989; Watanabe *et al*., 1992; Jansen *et al*., 2000; McGirt *et al*., 2003). If a brain lesion shows contrast medium enhancement in CT or MRI, the biopsy is usually directed to this area, assuming that the likelihood of highest malignancy is localized within the area of blood–brain barrier disruption (Chandrasoma *et al*., 1989). Serial biopsies of patients undergoing craniotomy for malignant gliomas, however, revealed infiltrating tumour cells more than 3 cm distant from the contrast-enhancing tumour margin (Burger *et al*., 1988). Furthermore, about 80% of the tumour relapses occur within a 2-cm margin from the enhancing tumour location (Wallner *et al*., 1989; Oppitz *et al*., 1999). A comparison of biopsy results in gliomas with histological analysis of the resected tumour demonstrated that all inaccurate biopsies were taken from MR-enhancing lesions (McGirt *et al*., 2003). These data emphasize that enhancement of contrast material alone is not a reliable parameter for tumour delineation. In our study, only 10 of 26 biopsies containing cellular tumour tissue showed contrast enhancement on MRI.

A more difficult clinical situation is to target an appropriate area for biopsy if brain lesions are characterized by abnormalities on T2-weighted MRI only and no sign of blood–brain barrier disruption is present. It is well known that in low-grade gliomas tumour tissue might be indistinguishable from normal brain parenchyma on CT and MRI (Kelly *et al*., 1987). Our data clearly demonstrate that in biopsies taken from brain areas with increased signal on T2-weighted FLAIR sequences tumour tissue was only found in approximately 50%.

Other MR techniques, such as magnetic resonance spectroscopy (MRS) and diffusion-weighted MRI (dwMRI), have been used to gain additional information in gliomas. Few data on the potential of MRS for the identification of the tumour extent are available and image co-registration of MRS data for neuronavigated or stereotactic biopsies is problematic (Vigneron *et al*., 2001; Pirzkall *et al*., 2002).

The utility of dwMRI has been mainly focused on the characterization of intracranial neoplasms by the apparent diffusion coefficient (ADC). In most studies no improvement was found for the non-invasive differentiation between tumour tissue and peritumoral brain tissue by using the ADC in patients with cerebral gliomas (Castillo *et al*., 2001; Stadnik *et al*., 2001; Provenzale *et al*., 2004; Pauleit *et al*., 2004). More recently, different authors have attempted to use diffusion-tensor metrics of dwMRI such as fractional anisotropy (FA) for characterization of different tissue components but inconsistent results have been reported. Lu and colleagues reported that diffusion-tensor MR metrics may enable the differentiation of tumour-infiltrated oedema from vasogenic oedema by introducing a tumour infiltration index (Lu *et al*., 2004). In contrast, Provenzale and colleagues found no significant difference among presumed tumour-infiltrated oedema and vasogenic oedema but found a significant difference of FA in normal-appearing white matter among patients with gliomas and meningiomas (Provenzale *et al*., 2004). However, in both studies FA revealed a large overlap for presumed vasogenic oedema in meningiomas and tumour-infiltrated oedema in gliomas, and histological confirmation was not performed in any case. Therefore, the conclusions drawn from those studies remain speculative to date.

Because of the well-known limitations of MRI for accurate assessment of the tumour extent, attempts have been made to incorporate metabolic imaging into the diagnostics and treatment planning of brain tumours. Several studies have shown that PET-guided stereotactic brain biopsy based on either MET PET or FDG PET increases the diagnostic yield and accuracy in finding tumour tissue compared with anatomical imaging only (Levivier *et al*., 1995; Massager *et al*., 2000; Pirotte *et al*., 2003, 2004). Recently, Pirotte and colleagues compared FDG PET and MET PET for PET-guided biopsy of gliomas and found that MET PET was superior to FDG PET (Pirotte *et al*., 2004). Depending on the radiotracer used, various molecular processes can be visualized by PET, most of them relating to increased cell proliferation within gliomas (for review see Jacobs *et al*., 2002).

The most common PET tracer FDG has a strong dependence on tumour grade (Janus *et al*., 1993) but has proved to be of little use in the definition of low-grade gliomas (Goldman *et al*., 1996). Previous studies using the 11C-labelled MET have also shown that the accumulation of radiolabelled amino acids spreads beyond the tumour margins as defined by CT and MRT (Bergstrom *et al*., 1983; Mosskin *et al*., 1989; Ogawa *et al*., 1993). However, an exact correlation of imaging findings in MRI, metabolic changes of amino acid uptake and histological tumour spread in these heterogeneous tumours has not yet been performed.

FET is one of the first 18F-labelled amino acids that can be produced in large amounts for clinical purposes and fulfils all

requirements for establishment in routine clinical practice, like the widely used FDG (Wester *et al*., 1999; Hamacher *et al*., 2002). The burden of radiation is low, with an effective dose of approximately 3 mSv per examination (Pauleit *et al*., 2003) and the whole brain can be examined in 20 min. FET shows no metabolic degradation in human plasma and tracer concentration in the brain and brain tumours remains rather stable 15 min after injection. A variable imaging period may be chosen between 15 min after injection and 60 min after injection or even later, which allows high patient throughput and cost-effectiveness. Furthermore, it has been shown in animal experiments that FET, in contrast to MET and FDG, exhibits low uptake in non-neoplastic inflammatory cells and in inflammatory lymph nodes, which promises higher specificity for the detection of tumour cells (Kaim *et al*., 2002; Rau *et al*., 2002).

One shortcoming of our study is the fact that, for ethical reasons, biopsies could only be taken from brain areas that appeared abnormal on MRI and/or FET PET images. Therefore, the infiltrative nature of the gliomas into normal brain and the presence of tumour foci in regions remote from abnormalities in MRI and PET may have been missed. This bias for FET- and MRI-positive brain tissue might influence the overall accuracy calculations but does not influence the improved discrimination of tumour tissue from peritumoral brain tissue.

In conclusion, our data suggest that the combined use of MRI and FET PET significantly improves the accuracy of MRI for the distinction of cellular glioma tissue from peritumoral brain tissue. This may have considerable impact on target selection for diagnostic biopsies as well as for therapy planning in patients with cerebral gliomas. Combined MRI and FET PET diagnostics seems to be especially useful in brain lesions without blood–brain barrier disruption and widespread abnormalities in T2-weighted MRI. Based on this study, preoperative imaging of cerebral gliomas should include additional metabolic imaging with FET PET to decrease the risk of diagnostically inconclusive biopsies.

Acknowledgements

The authors wish to thank Michael Sabel, Jochen Textor and Jörn Risse for participation in the ROC analysis; Suzanne Schaden, Elisabeth Theelen, Barbara Elghahwagi and Gabriele Oefler for assistance in the patient studies; and Silke Grafmüler, Bettina Palm and Erika Wabbals for assistance in the radiosynthesis of FET. This work was supported by the Brain Imaging Center West (BICW). The MRI facility at the Institute of Medicine, Research Center Jülich was supported by the Bundesministerium für Bildung und Forschung Grant No. BMBF 01GO0104 (N. J. Shah and K. Zilles). Dirk Pauleit and Frank Floeth contributed equally to this work.

References

Bergstrom M, Collins VP, Ehrin E, Ericson K, Eriksson L, Greitz T, et al. Discrepancies in brain tumor extent as shown by computed tomography and positron emission tomography using [68Ga]EDTA, [11C]glucose, and [11C]methionine. J Comput Assist Tomogr 1983; 7: 1062–6.

Burger PC, Heinz ER, Shibata T, Kleihues P. Topographic anatomy and CT correlations in the untreated glioblastoma multiforme. Neurosurgery 1988; 68: 698–704.

Castillo M, Smith JK, Kwock L, Wilber K. Apparent diffusion coefficients in the evaluation of high-grade cerebral gliomas. AJNR Am J Neuroradiol 2001; 22: 60–4.

Chandrasoma PT, Smith MM, Apuzzo ML. Stereotactic biopsy in the diagnosis of brain masses: comparison of results of biopsy and resected surgical specimen. Neurosurgery 1989; 24: 160–5.

DeAngelis LM. Brain tumors. N Engl J Med 2001; 344: 114–23.

Goldman S, Levivier M, Pirotte B, Brucher JM, Wikler D, Damhaut P, et al. Regional glucose metabolism and histopathology of gliomas. A study based on positron emission tomography-guided stereotactic biopsy. Cancer 1996; 78: 1098–106.

Hamacher K, Coenen HH. Efficient routine production of the 18F-labelled amino acid O-2–18F fluoroethyl-L-tyrosine. Appl Radiat Isot 2002; 57: 853–6.

Heiss P, Mayer S, Herz M, Wester HJ, Schwaiger M, Senekowitsch-Schmidtke R. Investigation of transport mechanism and uptake kinetics of O-(2-[18F]fluoroethyl)-L-tyrosine in vitro and in vivo. J Nucl Med 1999; 40: 1367–73.

Herholz K, Holzer T, Bauer B, Schroder R, Voges J, Ernestus RI, et al. 11C-methionine PET for differential diagnosis of low-grade gliomas. Neurology 1998; 50: 1316–22.

Jansen EP, Dewit LG, van Herk M, Bartelink H. Target volumes in radiotherapy for high-grade malignant gliomas of the brain. Radiother Oncol 2000; 56: 151–6.

Jacobs AH, Dittmar C, Winkeler A, Garlip G, Heiss WD. Molecular imaging of gliomas. Mol Imaging 2002; 1: 309–35.

Janus TJ, Kim EE, Tilbury R, Bruner JM, Yung WK. Use of [18F]fluorodeoxyglucose positron emission tomography in patients with primary malignant brain tumors. Ann Neurol 1993; 33: 540–8.

Johnson PC, Hunt SJ, Drayer BP. Human cerebral gliomas: correlation of postmortem MR imaging and neuropathologic findings. Radiology 1989; 170: 211–7.

Kaim AH, Weber B, Kurrer MO, Westera G, Schweitzer A, Gottschalk J, et al. (18)F-FDG and (18)F-FET uptake in experimental soft tissue infection. Eur J Nucl Med Mol Imaging 2002; 29: 648–54.

Kaschten B, Stevenaert A, Sadzot B, Deprez M, Degueldre C, Del Fiore G, et al. Preoperative evaluation of 54 gliomas by PET with fluorine-18-fluorodeoxyglucose and/or carbon-11-methionine. J Nucl Med 1998; 39: 778–85.

Kelly PJ, Daumas-Duport C, Kispert DB, Kall BA, Scheithauer BW, Illig JJ. Imaging-based stereotaxic serial biopsies in untreated intracranial glial neoplasms. J Neurosurg 1987; 66: 865–74.

Kleihues P, Louis DN, Scheithauer BW, Rorke LB, Reifenberger G, Burger PC, et al. The WHO classification of tumors of the nervous system. J Neuropathol Exp Neurol 2002; 61: 215–25.

Langen KJ, Jarosch M, Muhlensiepen H, Hamacher K, Broer S, Jansen P, et al. Comparison of fluorotyrosines and methionine uptake in F98 rat gliomas. Nucl Med Biol 2003; 30: 501–8.

Levivier M, Goldman S, Pirotte B, Brucher JM, Baleriaux D, Luxen A, et al. Diagnostic yield of stereotactic brain biopsy guided by positron emission tomography with [18F]fluorodeoxyglucose. J Neurosurg 1995; 82: 445–52.

Lu S, Ahn D, Johnson G, Law M, Zagzag D, Grossman RI. Diffusion-tensor MR imaging of intracranial neoplasia and associated peritumoral edema: introduction of the tumor infiltration index. Radiology 2004; 232: 221–8.

Massager N, David P, Goldman S, Pirotte B, Wikler D, Salmon I, et al. Combined magnetic resonance imaging and positron emission tomography-guided stereotactic biopsy in brainstem mass lesions: diagnostic yield in a series of 30 patients. J Neurosurg 2000; 93: 951–7.

McGirt MJ, Villavicencio AT, Bulsara KR, Friedman AH. MRI-guided stereotactic biopsy in the diagnosis of glioma: comparison of biopsy and surgical resection specimen. Surg Neurol 2003; 59: 277–81.

Messing-Junger AM, Floeth FW, Pauleit D, Reifenberger G, Willing R, Gartner J, et al. Multimodal target point assessment for stereotactic biopsy in children with diffuse bithalamic astrocytomas. Childs Nerv Syst 2002; 18: 445–9.

Mosskin M, von Holst H, Bergstrom M, Collins VP, Eriksson L, Johnstrom P, et al. Positron emission tomography with 11C-methionine and computed tomography of intracranial tumours compared with histopathologic examination of multiple biopsies. Acta Radiol 1987; 28: 673–81.

Mosskin M, Ericson K, Hindmarsh T, von Holst H, Collins VP, Bergstrom M, et al. Positron emission tomography compared with magnetic resonance imaging and computed tomography in supratentorial gliomas using multiple stereotactic biopsies as reference. Acta Radiol 1989; 30: 225–32.

Ogawa T, Shishido F, Kanno I, Inugami A, Fujita H, Murakami M, et al. Cerebral glioma: evaluation with methionine PET. Radiology 1993; 186: 45–53.

Oppitz U, Maessen D, Zunterer H, Richter S, Flentje M. 3D-recurrence-patterns of glioblastomas after CT-planned postoperative irradiation. Radiother Oncol 1999; 53: 53–7.

Pauleit D, Floeth F, Herzog H, Hamacher K, Tellmann L, Muller HW, et al. Whole-body distribution and dosimetry of O-(2-[18F]fluoroethyl)-L-tyrosine. Eur J Nucl Med Mol Imaging 2003; 30: 519–24.

Pauleit D, Langen KJ, Floeth F, Hautzel H, Riemenschneider MJ, Reifenberger G, et al. Can the apparent diffusion coefficient be used as a noninvasive parameter to distinguish tumor tissue from peritumoral tissue in cerebral gliomas. J Magn Reson Imaging 2004; 20: 758–64.

Pirotte B, Goldman S, Salzberg S, Wikler D, David P, Vandesteene A, et al. Combined positron emission tomography and magnetic resonance imaging for the planning of stereotactic brain biopsies in children: experience in 9 cases. Pediatr Neurosurg 2003; 38: 146–55.

Pirotte B, Goldman S, Massager N, David P, Wikler D, Vandesteene A, et al. Comparison of 18F-FDG and 11C-methionine for PET-guided stereotactic brain biopsy of gliomas. J Nucl Med 2004; 45: 1293–8.

Pirzkall A, Nelson SJ, McKnight TR, Takahashi MM, Li X, Graves EE, Verhey LJ, et al. Metabolic imaging of low-grade gliomas with three-dimensional magnetic resonance spectroscopy. Int J Radiat Oncol Biol Phys 2002; 53: 1254–64.

Provenzale JM, McGraw P, Mhatre P, Guo AC, Delong D. Peritumoral brain regions in gliomas and meningiomas: investigation with isotropic diffusion-weighted MR imaging and diffusion-tensor MR imaging. Radiology 2004; 232: 451–60.

Rau FC, Weber WA, Wester HJ, Herz M, Becker I, Kruger A, et al. O-(2-[(18)F]Fluoroethyl)- L-tyrosine (FET): a tracer for differentiation of tumour from inflammation in murine lymph nodes. Eur J Nucl Med Mol Imaging 2002; 29: 1039–46.

Stadnik TW, Chaskis C, Michotte A, Shabana WM, van Rompaey K, Luypaert R, et al. Diffusion-weighted MR imaging of intracerebral masses: comparison with conventional MR imaging and histologic findings. AJNR Am J Neuroradiol 2001; 22: 969–76.

Vigneron D, Bollen A, McDermott M, Wald L, Day M, Moyher-Noworolski S, et al. Three-dimensional magnetic resonance spectroscopic imaging of histologically confirmed brain tumors. Magn Reson Imaging 2001; 19: 89–101.

Wallner KE, Galicich JH, Krol G, Arbit E, Malkin MG. Patterns of failure following treatment for glioblastoma multiforme and anaplastic astrocytoma. Int J Radiat Oncol Biol Phys 1989; 16: 1405–9.

Watanabe M, Tanaka R, Takeda N. Magnetic resonance imaging and histopathology of cerebral gliomas. Neuroradiology 1992; 34: 463–9.

Weber WA, Wester HJ, Grosu AL, Herz M, Dzewas B, Feldmann HJ, et al. O-(2-[18F]fluoroethyl)-L-tyrosine and L-[methyl-11C]methionine uptake in brain tumours: initial results of a comparative study. Eur J Nucl Med 2000; 27: 542–9.

Wester HJ, Herz M, Weber W, Heiss P, Senekowitsch-Schmidtke R, Schwaiger M, et al. Synthesis and radiopharmacology of O-(2-[18F] fluoroethyl)-L-tyrosine for tumor imaging. J Nucl Med 1999; 40: 205–12.

Wong TZ, van der Westhuizen GJ, Coleman RE. Positron emission tomography imaging of brain tumors. Neuroimaging Clin North Am 2002; 12: 615–26.